

## Dielectric signatures of adsorbed and salty liquid water at the Phoenix landing site, Mars

David E. Stillman<sup>1</sup> and Robert E. Grimm<sup>1</sup>

Received 1 April 2011; revised 16 June 2011; accepted 23 June 2011; published 15 September 2011.

[1] The real part of the dielectric permittivity of the Martian regolith was measured by the Thermal and Electrical Conductivity Probe (TECP) on the Phoenix lander. We interpret these data using laboratory measurements of permittivity as a function of H<sub>2</sub>O and salt content, soil type, and temperature. Due to variability in sensor coupling, we focus on data taken at one locality (“Vestri”) three separate times, spanning multiple sols. A daytime increase in permittivity suggests progressive melting of a heterogeneous, disconnected, salty ice with a eutectic temperature of ~239 K, which is close to the eutectic temperatures of NaClO<sub>4</sub> or MgCl<sub>2</sub>. We found no evidence for Mg(ClO<sub>4</sub>)<sub>2</sub>. NaClO<sub>4</sub> and MgCl<sub>2</sub> are consistent with precipitation by freezing following a prior epoch of high obliquity. The evaporation of diurnal briny meltwater is inhibited by surface tension in small pores. An increase in permittivity occurred on the night of sol 70 that coincided with surface frost and measurement of a decrease in atmospheric water vapor. The permittivity jump can be matched by an increase in adsorbed H<sub>2</sub>O from ~1 monolayer to 3 monolayers in an analog soil with a Viking-like specific surface area (17 m<sup>2</sup>/g). However, the amount of adsorbed H<sub>2</sub>O is an order of magnitude larger than that inferred to have precipitated during the night. We suggest that the electrical signature of adsorbed water on Mars is stronger than we measured in the laboratory, possibly due to radiation damage of the regolith.

**Citation:** Stillman, D. E., and R. E. Grimm (2011), Dielectric signatures of adsorbed and salty liquid water at the Phoenix landing site, Mars, *J. Geophys. Res.*, 116, E09005, doi:10.1029/2011JE003838.

### 1. Introduction

[2] Phoenix landed on 25 May 2008 in Vastitas Borealis, Mars, at 68.219°N, and operated for 152 sols. Water ice was predicted to lie within tens of centimeters of the surface and was indeed found at an average depth of 4.25 cm [Arvidson *et al.*, 2009; Mellon *et al.*, 2009]. Salts including perchlorates were discovered in the regolith [Hecht *et al.*, 2009]. Liquid saline water droplets are believed to have formed via salt deliquescence on a landing strut of the spacecraft [Rennó *et al.*, 2009]. Phoenix also found a significant diurnal exchange of H<sub>2</sub>O between the atmosphere and regolith, where H<sub>2</sub>O vapor pressure and relative humidity were 1.8 Pa and 5–10% during the day and ~0.03 Pa and near 100% at night, respectively [Zent *et al.*, 2010]. Atmospheric H<sub>2</sub>O also declines substantially before either the surface or atmosphere has cooled to the frost point, suggesting that the regolith may be adsorbing H<sub>2</sub>O [Zent *et al.*, 2010].

[3] This paper furthers the interpretation of Thermal and Electrical Conductivity Probe (TECP) dielectric permittivity measurements by comparing them to laboratory data. The

TECP, an instrument on the Microscopy, Electrochemistry, and Conductivity Analyzer (MECA), was mounted on the robotic arm of Phoenix so that measurements of the top 15 mm of the subsurface could be made. This instrument measured relative humidity, thermal conductivity, volumetric heat capacity, temperature, electrical conductivity at 1 kHz, and dielectric permittivity at 6.25 MHz [Zent *et al.*, 2009]. Hereafter we refer to the real part of the relative dielectric permittivity simply as permittivity  $\epsilon'$ . The conductivity and permittivity were to be used to detect and quantify the population of mobile H<sub>2</sub>O molecules in the regolith.

### 2. Background

[4] The TECP consists of four 15 mm needles, each separated by 7 mm. To measure permittivity, an 8 MHz voltage square wave is applied to a 300  $\Omega$  resistor and capacitor that are in series [Zent *et al.*, 2009; D. Cobos, personal communication, 2011]. The capacitor is created by the third and fourth needles of the TECP with the dielectric being the material in between the two needles. The TECP measures the time required to charge the capacitor created by these two needles. The permittivity is measured at an effective frequency of 6.25 MHz [Zent *et al.*, 2009; D. Cobos *et al.*, TECP calibration report, 2008, [http://pds-geosciences.wustl.edu/geo/phx-m-meca-2-niedr-v1/phxmecc\\_0xxx/calibration/meca\\_tecp\\_calib\\_report.pdf](http://pds-geosciences.wustl.edu/geo/phx-m-meca-2-niedr-v1/phxmecc_0xxx/calibration/meca_tecp_calib_report.pdf)]. The analog to digital conversion (ADC output) of this charging

<sup>1</sup>Department of Space Studies, Southwest Research Institute, Boulder, Colorado, USA.

time is returned to Earth. The ADC output value is then corrected for temperature based on air-calibration measurements done on Mars. It is then converted into the real part of the relative dielectric permittivity (the imaginary part of the relative dielectric permittivity cannot be determined as only the charging time is returned), using an empirical calibration formula based on prelaunch tests [Zent *et al.*, 2009; D. Cobos *et al.*, TECP calibration report, 2008]. These tests were minimal: only four permittivities were measured (1, 8, 11, and 20) [Zent *et al.*, 2009] and none lie within the measured range observed on Mars ( $\epsilon' = 2-4$ ). The three largest permittivities used for the empirical calibration formula vary by as much as 8% compared to their expected or nominal values [Zent *et al.*, 2009]. The empirical calibration formula is a third-order polynomial, i.e., four parameters were fit exactly to four observations. Formal confidence limits are effectively unbounded with so few data.

[5] In addition to the overall scaling, temperature calibrations are necessary. The permittivity of Martian air should be very close to unity, but varied from 0.2 to 0.5 over 194–247 K, respectively. This correction to in situ data can, however, be performed to high accuracy (0.01 permittivity units). We assume this calibration applies to the TECP measurements in the regolith. Furthermore, one of the laboratory calibration standards was measured 9 K above the others [Zent *et al.*, 2009]. All told, relative differences of a few tenths of a permittivity unit—comparable to Mars-observed excursions of interest—can be introduced by different fittings of the calibration data and its temperature dependence.

[6] The permittivity measurements are also affected by variable coupling of the TECP to the ground. Void spaces due to incomplete insertion, complete insertion with partial retraction, or lateral movement will cause a decrease in permittivity. Conversely, over-insertion will increase the regolith relative density and hence permittivity. These variations are ubiquitous throughout the data at the nine different locations where the TECP was inserted into the ground. Although the local soil variations cannot be determined a priori, the effects can be corrected a posteriori, in a relative sense, where long time series are available.

[7] The TECP electrical conductivity always measured an open circuit (i.e., the effective conductivity was less than the lower limit of the instrument,  $0.2 \mu\text{S m}^{-1}$ ). This indicates that conduction currents are small and were possibly completely cut off by air gaps between the needles and the soil [Zent *et al.*, 2010]. Although the source signal was at 1 kHz, there is no discussion by D. Cobos *et al.* (TECP calibration report, 2008) or Zent *et al.* [2009] about displacement currents, so we neglect any analysis of AC conductivity. As determined by our laboratory experiments, the latter is generally too small to have been detected by TECP anyway.

[8] Zent and coworkers interpreted the TECP permittivity data and recognized “several puzzling signals and an overnight increase in permittivity in the latter half of the mission contemporaneous with H<sub>2</sub>O adsorption.” They used the Topp equation [Topp *et al.*, 1980] to estimate the amount of nighttime adsorbed water, but described their own quantitative results as “implausible.” This is mostly (neglecting measurement and calibration errors) because the Topp equation cannot accurately predict water content in fine-grained soils [Rubin and Hubbard, 2005, and references

therein]. We now understand this to be due to different dielectric signatures of H<sub>2</sub>O [Stillman *et al.*, 2010]: the Topp equation is based on the dielectric relaxation of liquid water in coarse and medium-textured soils, whereas adsorbed water, with different relaxations, dominates in fine-grained soils. In this paper, we extend the initial findings of Zent *et al.* [2010] using these new concepts and our own laboratory measurements of the temperature-dependent permittivity of Mars-analog materials.

### 3. Permittivity Laboratory Data

[9] We measured the permittivity of Mars-analog samples over a frequency range of 1 mHz – 1 MHz using a Solartron 1260 impedance analyzer with a 1296 dielectric interface and temperature range of 181–300 K. Water content was varied from 1 monolayer (ML) to a fully saturated pore space, using numerous silicates (JSC Mars-1 [Allen *et al.*, 1997], JSC-1 [McKay *et al.*, 1997], sand, smectite clay, and controlled pore glass), with different salt types (CaCl<sub>2</sub>, NaCl, KCl, MgSO<sub>4</sub>, Mg(ClO<sub>4</sub>)<sub>2</sub>, MgCl<sub>2</sub>, and NaClO<sub>4</sub>) and various salt-solution concentrations [see Stillman *et al.*, 2010]. All samples were first dried in a thermal-vacuum chamber for at least a day. The sample was weighed immediately after removal from the chamber and the requisite amount of water was mechanically mixed into the sample. We assumed that “dry” samples acquired ~1 ML of adsorbed H<sub>2</sub>O from the relatively low-humidity laboratory atmosphere. The number of extra ML was taken to be the added volumetric water content divided by the specific surface area. See Grimm *et al.* [2008] and Stillman *et al.* [2010] for experimental procedures and related data.

[10] Below infrared frequencies, polar molecules and spatially bounded ions show dielectric relaxations in which the permittivity always decreases with increasing frequency. Temperature dependence of dielectric relaxations is well described by an Arrhenius equation [Kauzmann, 1942] with the dielectric relaxation frequency decreasing with temperature. Therefore, “high” frequency (>1 MHz) behaviors can be brought into our bandwidth simply by measuring at lower temperature. Conversely, it is straightforward to extrapolate our measurements that go up to 1 MHz to the TECP frequency of 6.25 MHz [Stillman and Grimm, 2011].

[11] For dry minerals and rocks, the permittivity is dominated by bulk density  $\rho$  due to electronic polarization:  $\epsilon' = (1.93 \pm 0.17)^\rho$  [Olhoeft and Strangway, 1975]. This relationship is not temperature dependent at Martian temperatures, although it cannot be applied to any water-bearing material, as water is a polar molecule. On the other hand, if >1 ML of adsorbed water is present, frequency and temperature dependence will occur [McCafferty and Zettlemoyer, 1971]. Permittivity increases with temperature (Figure 1). The permittivity also increases as the number of adsorbed water monolayers increases from one to three, due to a low-frequency dispersion [e.g., McCafferty and Zettlemoyer, 1971; Shahidi *et al.*, 1975; Jonscher, 1978; Stillman *et al.*, 2010]. Even at only 3 ML, frozen saline (>1 M) solutions enhance permittivity over deionized (DI) water [Stillman and Grimm, 2011]. Once 3 ML of water are adsorbed, additional water forms liquid water or ice depending on temperature and salt content [Anderson and Tice, 1973; Asay and Kim, 2005; Stillman *et al.*, 2010].

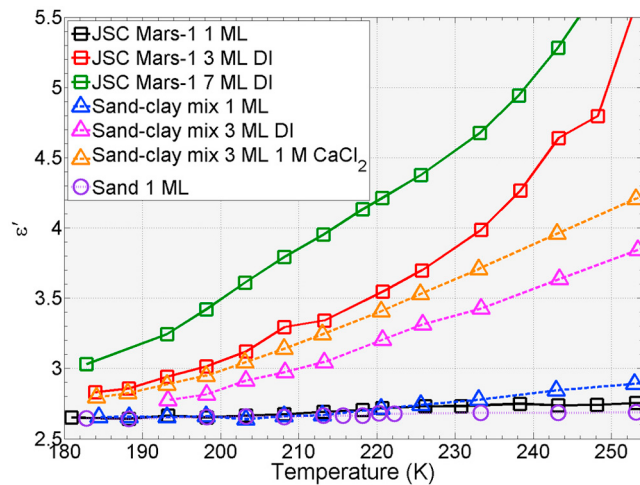


**Figure 1.** Temperature dependence of the permittivity at 6 MHz of JSC Mars-1 (specific surface area  $A_s = 106 \text{ m}^2/\text{g}$ ), a sand-clay mixture ( $A_s = 17 \text{ m}^2/\text{g}$ ), and a fine-grained sand ( $A_s = 0.1 \text{ m}^2/\text{g}$ ) with 1, 3, and 7 monolayers (ML) of adsorbed water. Deionized water (DI) or 1 M  $\text{CaCl}_2$  solution were added to samples with  $>1$  ML. Permittivity increases with the number of ML, salt concentration  $\geq 1$  M, and generally with the  $A_s$  [see also *Stillman and Grimm, 2011*]. Beyond 3 ML there is little change in temperature dependence because additional  $\text{H}_2\text{O}$  is in the form of ice, which simply shifts the permittivity values up. Permittivity has been corrected for bulk density by matching dry samples at low temperature.

This ice or water also increases the permittivity (both water and ice have a larger permittivity than air) but differently than the underlying adsorbed  $\text{H}_2\text{O}$  (Figure 1).

[12] Liquid water can exist in the subsurface and surface (under special conditions) of Mars due to salts with low eutectic temperatures [*Rennó et al., 2009; Chevrier et al., 2009*]. At the Phoenix landing site, numerous cations ( $\text{Mg}^{2+} > \text{Na}^+ > \text{Ca}^{2+} > \text{K}^+$ ) and anions ( $\text{ClO}_4^- > \text{Cl}^-$ ) have been detected [*Hecht et al., 2009*]. Geochemical modeling [*Marion et al., 2010*] shows that these ions likely form low-melting-temperature salts such as sodium perchlorate  $\text{NaClO}_4$  (eutectic temperature  $236 \pm 1 \text{ K}$  [*Chevrier et al., 2009*] or  $239 \text{ K}$  as suggested by *Linke [1965]*, *Chretien and Kohlmuller [1966]*, and *Marion et al. [2010]*; see Figure 2), magnesium chloride  $\text{MgCl}_2$  (eutectic temperature  $240 \text{ K}$ ), and magnesium perchlorate  $\text{Mg}(\text{ClO}_4)_2$  (eutectic temperature  $206 \text{ K}$  [*Dobrynina et al., 1980; Pestova et al., 2005*] or  $216.0 \pm 0.2 \text{ K}$ ; see Figure 2 and Appendix A). Note that all of these compounds are coordinated with  $\text{H}_2\text{O}$ , thus forming salt hydrates.

[13] Electrical-properties measurements can precisely determine the eutectic temperature of a salt solution because the permittivity (from  $\sim 100 \text{ kHz} - 1 \text{ GHz}$ ) and DC electrical conductivity increase significantly when the frozen solution is melted (Figure 2 and Appendix A [*Grimm et al., 2008; Stillman et al., 2010*]). A jump in the conductivity only occurs if the liquid portion is electrically connected when the temperature is increased through the eutectic temperature [e.g., *Stillman et al., 2010*]. However, a jump in the permittivity always occurs. If the salty solution is below its

eutectic composition, but above its eutectic temperature then permittivity will increase progressively with temperature. In a eutectic composition there will be no further change in permittivity. It should also be noted that the initial steep slope in permittivity versus temperature is due to premelting [*Grimm et al., 2008; Stillman et al., 2010*] (see *Dash et al. [2006]* for a review). The eutectic temperature is at the slope break between pre- and post-melting (e.g., Figure 2).

[14] Our measurements, along with those of others [e.g., *Bittelli et al., 2003*], show hysteresis in the permittivity versus temperature caused by supercooling of brine. As supercooling is metastable, the magnitude of hysteresis varies from sample to sample. Our measurements are always reported during warming, as this leads to reproducible data, but it must be recognized that TECP measurements are reported during both warming and cooling, and can therefore be hysteretic.

#### 4. TECP Data

[15] Permittivity data sets longer than  $1/2$  a sol are needed to set control points to correct for variable probe-regolith coupling. There are only three data records of sufficient length and they are all at the Vestri site (Figure 3). Vestri was located behind (from the lander's perspective) a large rock (Headless) and had an ice table  $6.5 \text{ cm}$  beneath the surface [*Zent et al., 2010*]. We adopted the first insertion (Vestri-1, Sol 46–47) as the datum because the dry permittivities most closely matched our laboratory measurements. We shifted the permittivity from the second (Vestri-2, Sol 54–56) and third (Vestri-3, Sol 69–71) insertions down by 1 and 0.1 dimensionless permittivity units, respectively, to match all three data sets at approximately 6.2 and 20.3 h Local Mean Solar Time (LMST; Figure 4, top). Sol 71 data were shifted an additional 0.25 to align with sol 69 and 70. To further aid in the interpretation of the temperature-dependent permittivity, subsurface temperatures measured in needle 4 of the TECP (Figure 4, bottom) were interpolated to the exact times of the permittivity measurements.

[16] The data shift is not a true calibration, but is a correction for interpretation purposes. If we neglect the insertion errors, the Vestri data would suggest a bulk density range of  $1.33 - 1.87 \text{ g/cm}^3$  within  $\sim 12 \text{ cm}$ , while all TECP measurements would suggest a range of  $1.05$  (Vestri sol 122) –  $2.11$  (Rosy Red 111)  $\text{g/cm}^3$  within  $\sim 75 \text{ cm}$ . There is no evidence from other Phoenix investigations for a factor

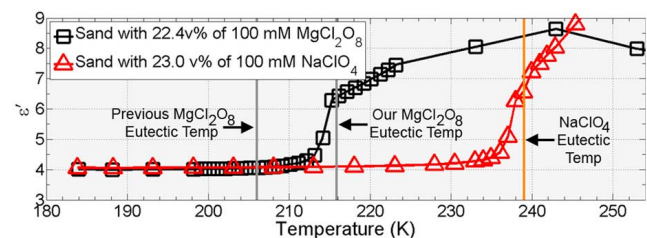


**Figure 2.** Permittivity temperature dependence of two perchlorate salts mixed with sand at nearly full volume saturation. As salty ice warms through its eutectic temperature, the dielectric permittivity increases continuously due to increasing liquid  $\text{H}_2\text{O}$  fraction. The initial sharp rise is premelting, so the eutectic is at the slope break.

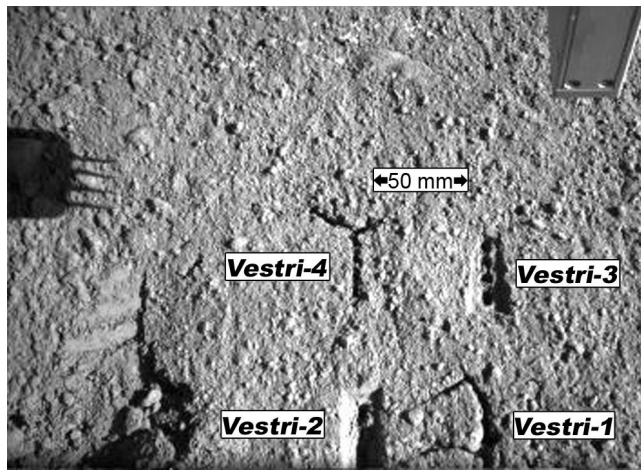


**Figure 3.** TECP insertion points Vestri-1 (Sol 46–47), Vestri-2 (Sol 54–56), Vestri-3 (Sol 69–71), and Vestri-4 (Sol 122–123). TECP insertion packed down the regolith especially at Vestri-2 as is evident by the high pre-shifted permittivity values. Data at Vestri-4 were taken over two sols, but these data are too sparse to be used. TECP shadow is visible at upper left; permittivity was measured by the top two needles.

of two difference in soil density, so we treat these variations as insertion errors.

## 5. Results and Interpretation

### 5.1. Vestri-1

[17] At the warmest part of the day, the permittivity is 0.2 units above its value during the coldest part of the night at Vestri-1 (Figures 4 and 5). It is unclear exactly when the change in permittivity occurs due to lack of data between 6.95 and 11.9 LMST, but the decrease in permittivity starts at 18.4 LMST when subsurface temperatures drop below 245 K. By 21.3 LMST at 222.5 K, the permittivity plateaus. The permittivity data concludes at 6.95 LMST at a subsurface temperature of 233.5 K and does not indicate a trend to a higher value of permittivity.

[18] We infer that these changes in permittivity that are directly correlated with temperature are caused by melting of salty ice during the day. Because the TECP data taken here were largely during cooling, there is the possibility of supercooling hysteresis. The data indeed hint at such hysteresis as the warming data at 6.95 LMST (233.2 K) on sol 47 have lower permittivity than the cooling data at similar temperature (Figure 5). Without the warming data and specific evidence of premelting, we can only limit the eutectic temperature of the salt-ice mixture to  $\geq 233.5$  K. Nonetheless, this shows that the daytime increase in permittivity is not

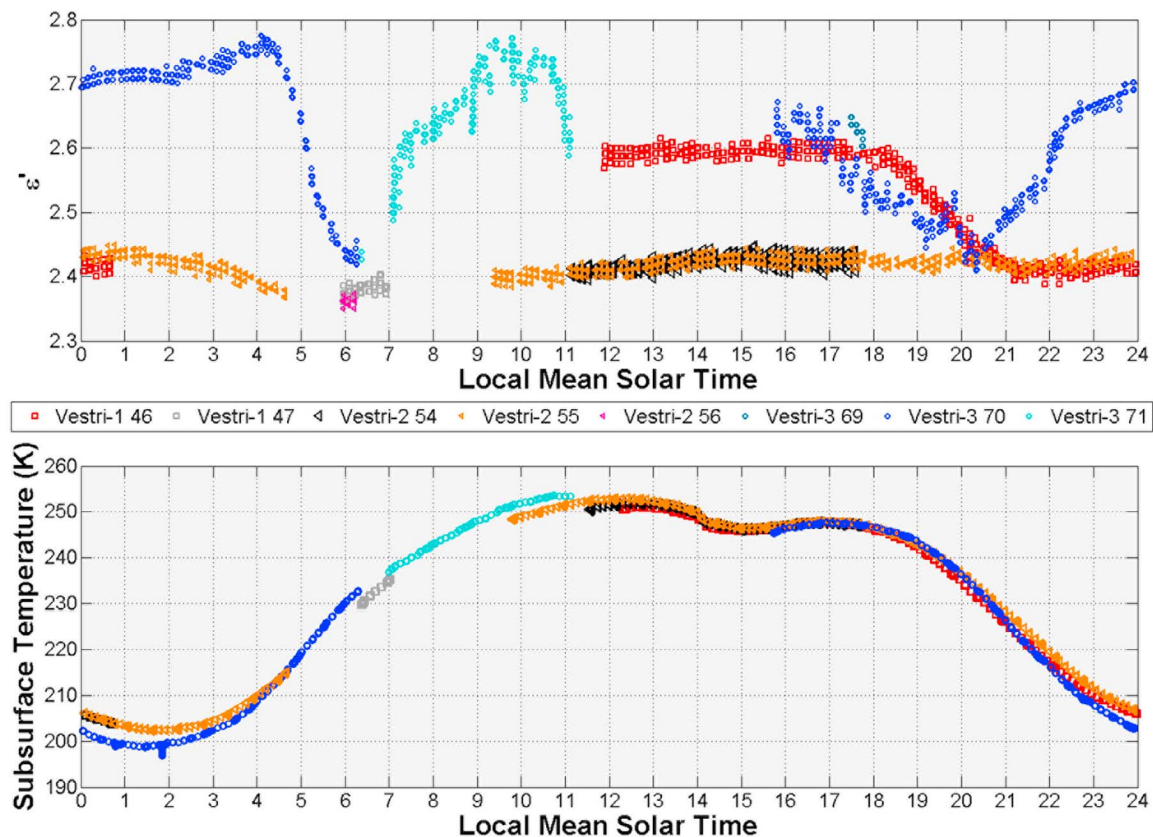


**Figure 4.** (top) TECP dielectric permittivity data as a function of Local Mean Solar Time (LMST), shifted to match Vestri-1 at 6.2 and 20.3 h. (bottom) Subsurface temperature (measured in needle 4) as a function of LMST at three slightly different locations at Vestri.

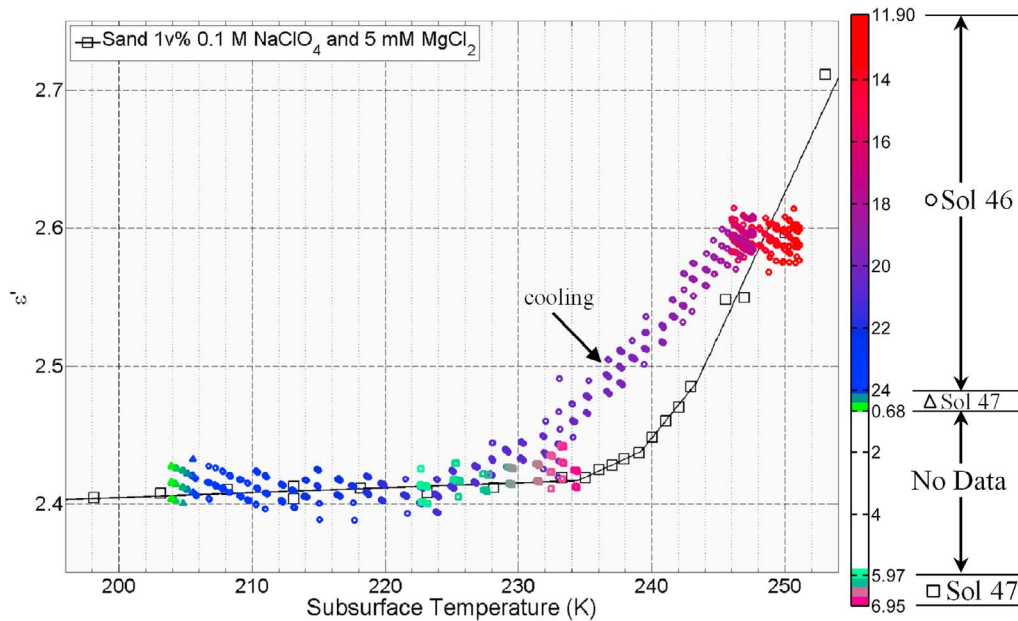


**Figure 5.** TECP permittivity of Vestri-1 as a function of temperature and time (symbol color) overlaid with our laboratory data of a fine-grained sand with 1 v% solution of 100 mM  $\text{NaClO}_4$  and 5 mM  $\text{MgCl}_2$ . This composition matches the visible onset of melting (pink dots near  $\epsilon' = 2.4$ ). No premelting is evident and the higher TECP permittivities are likely the result of supercooling hysteresis (laboratory measurements were made during warming, TECP during cooling).

due to  $\text{Mg}(\text{ClO}_4)_2$ , but instead possibly due to  $\text{NaClO}_4$  or  $\text{MgCl}_2$ . The plateau in permittivity from 246 to 251 K may be caused by a eutectic composition (there is no further melting) or it may have been caused by evaporation of some of the liquid portion.

[19] This conceptual model is supported by laboratory data of a fine-grained sand containing 1 v% of a frozen solution of 100 mM  $\text{NaClO}_4$  and 5 mM  $\text{MgCl}_2$  (Figure 5). This sample provides a good (albeit nonunique) match to the onset of the permittivity increase; hysteresis between the laboratory measurements and TECP is evident.

## 5.2. Vestri-3

[20] This is the most complicated permittivity time series: both the warmest part of the day and the coldest part of the night have permittivities 0.2–0.35 units above the minima (Figure 4). Zent *et al.* [2010] noted the two deep “V” shaped excursions in this data set and interpreted just the last part (22 LMST sol 70 – 4 LMST sol 71) of one of the V’s as caused by adsorbed water. We show below that two different mechanisms that operate during the day and night are the cause of the drop and subsequent rise of the V.

[21] Overall, the daytime data (Figure 6) behave similarly to Vestri-1. The minimum permittivity probably occurred between 6.4 and 7.1 LMST (233 and 237 K, respectively), when data were not collected. The permittivity increases sharply with time between 7.1 and 7.3 LMST, after which it still continues to increase but not as fast. We interpret this slope break as the pre-to-post eutectic melting transition, and therefore we can assign a eutectic temperature of  $\sim 239.2$  K. This is very near the eutectic temperature of both  $\text{NaClO}_4$  and  $\text{MgCl}_2$ . The gradual increase in permittivity with temperature above the eutectic temperature indicates

that melting is continuing and therefore the frozen mixture is not a eutectic composition. The permittivity decreases after 10.7 LMST (253 K), which may be a signature of evaporation.

[22] The Vestri-3 daytime trends were compared to a fine-grained sand with 2 v% of an  $\text{NaClO}_4$  eutectic (52 wt%) solution (Figure 6). The onset and sharp increase in permittivity are well matched, although the laboratory sample attains a higher permittivity upon complete melting and its permittivity begins to decrease due to evaporation above its eutectic temperature.

[23] A very different pattern evolved overnight at Vestri-3 (Figure 7). After linearly decreasing from 17 to 20.3 LMST (247 to 233 K, respectively), the permittivity begins increasing with decreasing temperature. The increase is  $\sim 0.3$  permittivity units at face value, but could be as large as 0.4 relative to the laboratory baseline. At 4.1 LMST temperatures rise quickly and permittivity falls back to its value from the previous evening. We interpret this cycle as the signature of water adsorbing and then desorbing off the regolith. Note that Zent and colleagues only considered the latter part of the adsorption (i.e., from a LMST of 22 to 4.1 with a 0.1 jump in permittivity).

[24] We compare this adsorption signature to laboratory experiments on two sand-clay mixtures: one with the same specific surface area ( $A_s = 17 \text{ m}^2/\text{g}$ ) as that inferred by Ballou *et al.* [1978] for Viking 1 trench samples, and the second with a surface area of  $1 \text{ m}^2/\text{g}$ . The Vestri-3 nighttime data are bounded by the Viking-analog material containing 1 ML and 3 ML of adsorbed water (Figure 7). The response of 3 ML of deionized water is slightly too small, whereas 3 ML of 1 M  $\text{CaCl}_2$  perfectly fits the data. Previous mea-

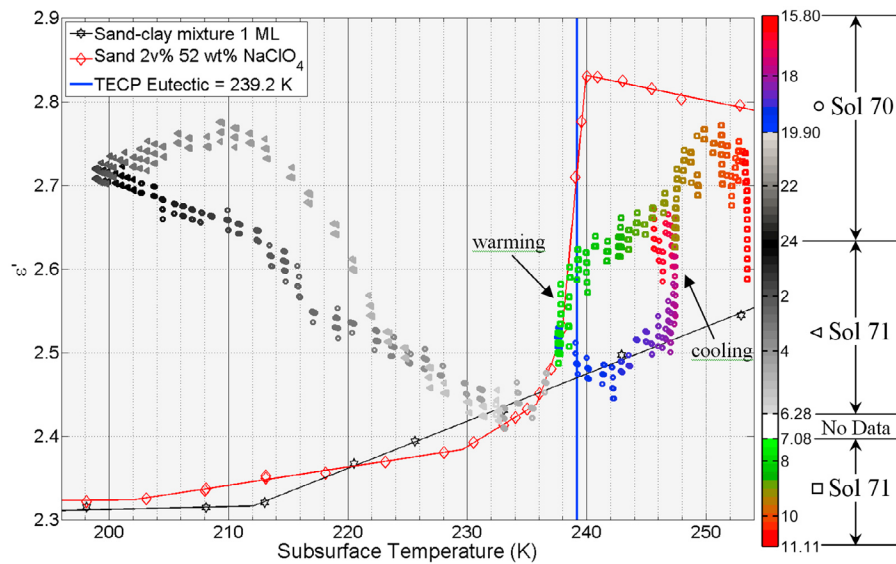


**Figure 6.** TECP daytime permittivity of Vestri-3 as a function of temperature (symbol color, nighttime data grayed out and are treated in Figure 7), overlaid with data from two laboratory samples. TECP warming data show initial steep rise and subsequent flattening of  $\epsilon'$  consistent with premelting, followed by progressive melting of ice with subeutectic salt concentration (compare to Figure 2). Evaporation may cause afternoon decrease in  $\epsilon'$  and subsequent cooling hysteresis. One monolayer of adsorbed water on a sand-clay mixture with specific surface area similar to that of Viking 1 regolith ( $17 \text{ m}^2/\text{g}$ ) yields an appropriate background. Premelting is well matched by a frozen solution of 2 v% of a 52 wt% (eutectic) concentration of  $\text{NaClO}_4$ , but diverges from TECP above the eutectic temperature.  $\text{MgCl}_2$  is an alternative salt as its eutectic temperature is also very close to the onset of melting in TECP. Note evaporation in the laboratory sample at higher temperatures.

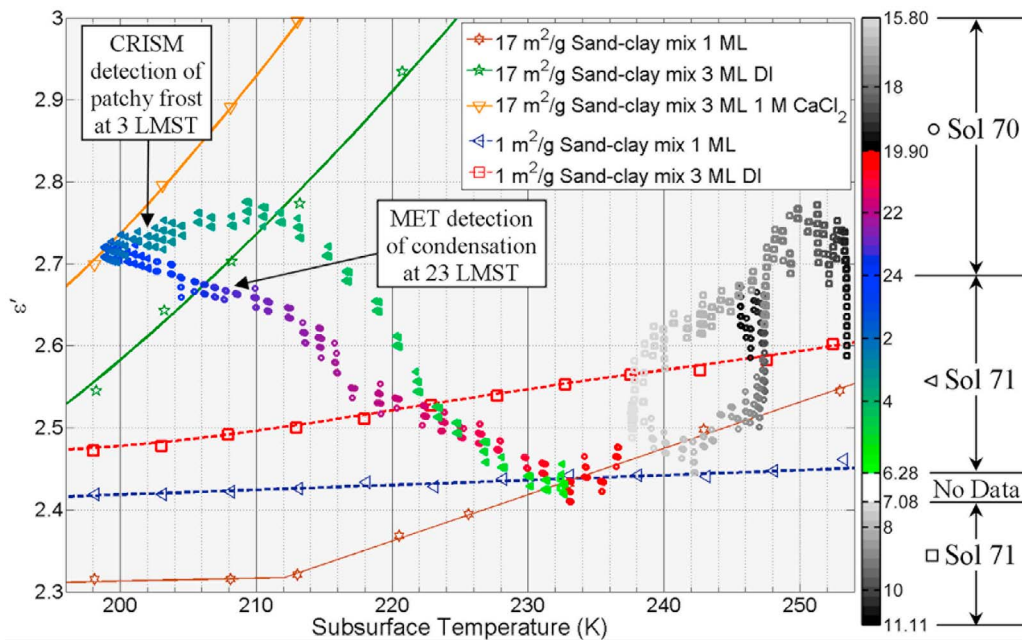


**Figure 7.** TECP permittivity of Vestri-3 as a function of temperature, overlaid with our laboratory data. The color scale is similar to Figure 6, but the nighttime adsorption of water is emphasized here. The TECP data are consistent with the addition of two  $\text{H}_2\text{O}$  ML between Sol 70, 20.3 LMST and Sol 71, 0.7 LMST, followed by desorption until Sol 71, 6.28 LMST. The magnitude of the jump in permittivity is best matched by a  $17 \text{ m}^2/\text{g}$  soil with 1 M of  $\text{CaCl}_2$  salt.  $\text{NaClO}_4$  is an alternative salt (see Figure 6), but lower surface area ( $1 \text{ m}^2/\text{g}$ ) clearly cannot match the observed excursion in permittivity or temperature dependence.

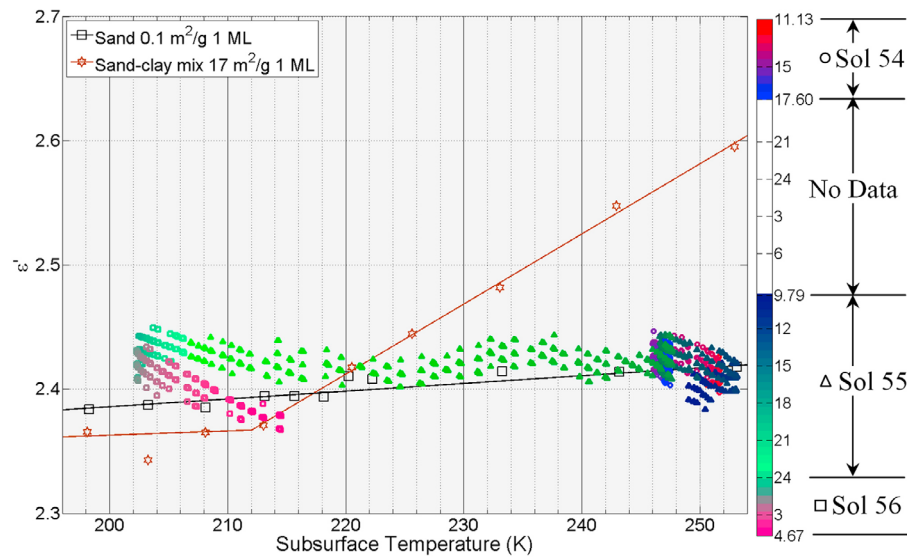


**Figure 8.** TECP permittivity of Vestri-2 as a function of temperature overlaid with our laboratory data of 1 H<sub>2</sub>O ML on samples with 17 and 0.1 m<sup>2</sup>/g. The flat temperature response of the TECP permittivity does not fit the higher surface area material that is required for adsorption at Vestri-3.

measurements have shown that Cl-bearing salts  $\geq 1$  M further increase the permittivity [Stillman and Grimm, 2011]. Note that the overall deviation due to the addition of two extra monolayers of H<sub>2</sub>O is more significant than the salt type and concentration. It is also clear that a material with smaller surface area does not produce a large change in dielectric constant due to adsorbed water. Note that additional H<sub>2</sub>O ML could be present as ice, but would not substantially affect the 6-MHz permittivity at this modest  $A_s$  and low temperature (see Figure 1).

### 5.3. Vestri-2

[25] The permittivity at Vestri-2 is temperature independent over nearly three days (Figure 8). Therefore, no salty solutions or adsorbed water were detected here within the TECP measuring volume. This indicates substantial lateral heterogeneity at scales of centimeters as melting of salty ice was detected at both Vestri-1 and Vestri-3. A laboratory measurement of a sand-clay mixture (17 m<sup>2</sup>/g) produces much more temperature dependence than is observed; instead this site seems to have a much lower surface area, e.g., 0.1 m<sup>2</sup>/g (Figure 8).

## 6. Discussion

### 6.1. Adsorbed Water

[26] Instruments other than TECP also detected changes in the H<sub>2</sub>O budget on sol 70–71 [Zent *et al.*, 2010; Tamppari *et al.*, 2010; Cull *et al.*, 2010]. Measurements by the Compact Reconnaissance Imaging Spectrometer for Mars (CRISM) indicated that between 15 LMST Sol 70 and 3 LMST Sol 71 atmospheric water vapor decreased by  $\sim 15$  precipitable (pr)  $\mu\text{m}$ , and surface frost was detected in the second measurement [Tamppari *et al.*, 2010]. The 2-m meteorological station (MET) mast and lidar on Phoenix indicated ground condensation at  $\sim 23$  LMST [Zent *et al.*,

2010]. Zent and coworkers estimated that cloud and frost formation left  $\leq 10$  pr  $\mu\text{m}$  to be adsorbed into the subsurface.

[27] The overnight increase in permittivity is unlikely to have been caused by frost for two reasons. First, the permittivity change is continuous with time and shows no jumps indicating rapid deposition. Second, the dielectric constant of ice at 6.25 MHz is smaller than that of semi-mobile adsorbed water, so more frost would be required than adsorbed water. Frost could have deposited just on the TECP needles, if their temperature was colder than that of the subsurface. The strong radial dependence of sensitivity would then strongly weight material near the electrode surfaces. However, numerical modeling (see methods in Appendix B) indicates that a 1-mm coating on the electrodes would require permittivity 25 (where ice has a permittivity of 3.15) to change from a background value of  $\sim 2.4$  to the measured value of  $\sim 2.7$ .

[28] Using the Topp equation, Zent *et al.* [2010] found that 10 pr  $\mu\text{m}$  could produce an increase in permittivity of 0.1 *only if the sample already contained 20% unfrozen water*. The calculation also resulted in a bulk permittivity  $\sim 10$ , which was twice as large as any permittivity observed by the TECP. We stated above that the Topp equation is not applicable to fine-grained soils at low saturation. Also recall that we interpret the nominal permittivity increase of  $\sim 0.3$  due to adsorbed water, which is three times larger than was adopted in the calculation by Zent and colleagues.

[29] Our laboratory measurements suggest that an additional 2 ML of H<sub>2</sub>O on a 17 m<sup>2</sup>/g soil can produce the required permittivity increase via a low-frequency dispersion. The TECP permittivity measurement is sensitive over a depth about equal to the probe length (Appendix B), so this additional water must occur to a depth of at least 15 mm. This is  $\sim 20$  times more water ( $\sim 200$  pr  $\mu\text{m}$  for a soil density of 1.5 g/cm<sup>3</sup>) than was inferred to have precipitated. Calibration errors could reduce the permittivity excursion to  $< 0.2$ .

Furthermore, the TECP response at the surface is approximately 1.4 times the depth-averaged value (Appendix B). Therefore, adsorbed water in the top few millimeters, on materials with higher surface area ( $\sim 100 \text{ m}^2/\text{g}$  [see *Pommerol et al.*, 2009]), could dominate the dielectric signature. Both of these effects could combine to reduce the required abundance of adsorbed  $\text{H}_2\text{O}$  by a factor of two. Our inference in the amount of water adsorbed during the night of sol 70–71 remains a factor of  $\sim 10$  larger than the amount of water inferred to have precipitated. If additional ice was precipitated in the subsurface, the difference is exacerbated. Note that  $\text{H}_2\text{O}$  vaporized from the ice table can be ruled out because the adsorption event was correlated with atmospheric changes, and the condensable  $\text{H}_2\text{O}$  from the ice table is  $< 0.01 \text{ pr } \mu\text{m}$  over the depth of the TECP probes anyway.

[30] The discrepancy could be resolved by passage of a humid air mass, heterogeneity in the specific surface area,  $\text{H}_2\text{O}$  transport due to TECP heating, or a dielectric response of adsorbed water in the Martian regolith that is much larger than measured in our laboratory experiments. We address these hypotheses in turn.

[31] *Zent et al.* [2010] used changes in the vertical column abundance of  $\text{H}_2\text{O}$  to infer that up to  $10 \text{ pr } \mu\text{m}$  were adsorbed by the regolith over sols 70–71. This assumes a stagnant air mass. Wind speeds averaged  $\sim 4 \text{ ms}^{-1}$  at the Phoenix site, but could have been faster at higher altitude and were from the east overnight, so water could be transported up to a few hundred km. Therefore, unusual ground or air properties for 10 km around the Phoenix site would have been required to adsorptively integrate  $\sim 100 \text{ pr } \mu\text{m}$  of  $\text{H}_2\text{O}$ . Although the Heimdal outer ejecta unit on which Phoenix landed is formed from fine-grained materials [*Heet et al.*, 2009], it seems unlikely that it would form a unique sink.

[32] Alternatively,  $\sim 10\%$  of the surface at the Phoenix site could have higher surface-area materials ( $17 \text{ m}^2/\text{g}$ ), with the remainder an order of magnitude or more lower (perhaps  $1 \text{ m}^2/\text{g}$ ), at least in the top few mm. This premise is supported by the observation of ice melting at Vestri-1 and Vestri-3 but not at Vestri-2. Furthermore, the frost on the night of sol 70 was patchy [*Tamppari et al.*, 2010; *Cull et al.*, 2010]. However, short-duration TECP data at “Sindr” on Sol 104 and “Rosy Red” on Sol 111 both suggest the presence of adsorbed water overnight, but they lack daytime data. Therefore, this hypothesis cannot be rigorously tested due to the lack of long duration TECP data after sol 70.

[33] Because both the thermal conductivity and permittivity experiments were run concurrently, heating at needle 1 could have caused redistribution of  $\text{H}_2\text{O}$ . An upper limit of a factor of  $\sim 1.8$  enhancement would follow if all of the  $\text{H}_2\text{O}$  around needle 1 to the radius of needle 3 were driven into the annulus between needles 3 and 4. As the actual enhancement is likely less, this hypothesis alone cannot solve the water discrepancy.

[34] We are left with the inference that  $\sim 10 \text{ pr } \mu\text{m}$  was adsorbed but the dielectric signal on Mars is larger than we measured in our laboratory. Either the dielectric strength of adsorbed water on Mars is at least several times larger than expected, or our laboratory conditions and procedures damp the response by the same factor. We can reject displacement of  $\text{H}_2\text{O}$  by  $\text{N}_2$  under ambient laboratory conditions using

simple Langmuir adsorption theory (BET theory is not applicable because  $\text{N}_2$  is supercritical). The ratio of surface sites occupied by water versus nitrogen is  $\theta_{\text{H}_2\text{O}}/\theta_{\text{N}_2} = K_{\text{H}_2\text{O}}P_{\text{H}_2\text{O}}/K_{\text{N}_2}P_{\text{N}_2}$ , where  $K$  is the equilibrium constant and  $P$  is the pressure. At 293 K, we have  $K_{\text{H}_2\text{O}} \sim 1 \text{ Pa}^{-1}$  and  $K_{\text{N}_2} \sim 10^{-7} \text{ Pa}^{-1}$ , derived from data of *Beck et al.* [2010] and *Zhou* [2002], respectively. This large difference is a consequence of the high dipole moment of  $\text{H}_2\text{O}$ . Taking the standard atmospheric pressure of  $\text{N}_2$  and 10% relative humidity for  $\text{H}_2\text{O}$ , we find  $\theta_{\text{H}_2\text{O}}/\theta_{\text{N}_2} \sim 10^4$ . A large ratio also results for  $\text{H}_2\text{O}$  over  $\text{O}_2$ . On Mars, co-adsorption of  $\text{CO}_2$  would weaken the dielectric strength (i.e., opposite the desired direction). Using both BET and Langmuir theory, we find  $\theta_{\text{H}_2\text{O}}/\theta_{\text{CO}_2} \sim 10^2\text{--}10^3$  for Mars. This is consistent with the measurements of *Zent and Quinn* [1995], who found that  $\text{H}_2\text{O}$  readily displaces  $\text{CO}_2$ .

[35] The surface of Mars experiences a form of “space weathering” from cosmic rays, solar flares, and ultraviolet irradiation (and their interactions with the atmosphere and regolith). This will impact electrical properties. The electrical conductivity of lunar soils was found to have a temperature dependence characteristic of amorphous semiconductors [*Olhoeft et al.*, 1974], which was interpreted as a consequence of radiation damage. Neutron radiation introduces dielectric relaxations in electronic semiconductors as carriers are heterogeneously affected in the space-charge region around the p-n junction [*Gregory and Gwyn*, 1974]. No experiments have been done to date specifically to assess the effects of radiation-induced surface damage on the dielectric properties of adsorbed water. However, there is no doubt that radiation-induced surface damage would change the distribution of activation energies for charge hopping and tunneling, which creates the broadband nature of the low-frequency dispersion [*Stillman et al.*, 2010, and references therein]. It is likely that the distribution of activation energies would be broadened via the damage, thereby increasing the permittivity at all frequencies.

## 6.2. Salty Meltwater

[36] We inferred from Vestri-3 that a salt with a eutectic temperature of  $\sim 239 \text{ K}$  was present in the soil. This eutectic temperature is near those of  $\text{NaClO}_4$  (239 K) and  $\text{MgCl}_2$  (240 K), but is much higher than that of  $\text{Mg}(\text{ClO}_4)_2$  (206 – 216 K, see Appendix A). As described above, we found no evidence for  $\text{Mg}(\text{ClO}_4)_2$ . Magnesium perchlorate would have to remain in a metastable supercooled-state for many hours through the night to avoid a detectable phase transition at the eutectic temperature.

[37] *Marion et al.* [2010] modeled the MECA geochemical results and found that the  $\text{NaClO}_4$  was the dominant salt followed by  $\text{MgCl}_2$  or  $\text{Mg}(\text{ClO}_4)_2$ , depending on whether the solution is frozen or evaporated, respectively. Therefore, our results suggest that the salts at the Phoenix site formed via freezing. In this scenario, liquid water was present, perhaps intermittently, during a prior epoch of high obliquity [e.g., *Jakosky et al.*, 2003]. Salts were leached from the soil or atmospherically deposited. Salt hydrates were formed by freezing as the obliquity decreased and insolation fell.

[38] The volume of the melt is very small. Using a permittivity power law mixing model [*Shivola*, 1999] with an exponent of 2.7 [*Shabtaie and Bentley*, 1994; *Stillman et al.*,

2010], we find that a change in permittivity by 0.2 at Vestri-1 and 3 could be caused by melting a volume of  $\sim 1.2\%$ . The overall melt fraction at the Phoenix site must be even smaller because there was no signature at Vestri-2. The calibration uncertainties described earlier would further lower this value. If a continuous melt between the TECP needles existed, it would have produced a detectable electrical conductivity at 1 kHz if both needles were in contact with the regolith. Therefore, the liquid most likely exists as disconnected blobs or stringers.

[39] Even 1% liquid is remarkable, as this must be produced in thaw-freeze cycles day after day during the summer, and probably year after year under the present climate conditions. Surface water will evaporate under contemporary Martian atmospheric conditions [e.g., *Haberle et al.*, 2001]. However, surface tension reduces the vapor pressure  $P$  according to the Kelvin equation [see *Fanale and Cannon*, 1979]:

$$P = P_0 \exp\left(\frac{-2V\gamma \cos \theta}{RT r}\right) \quad (1)$$

where  $P_0$  is the vapor pressure over a flat surface,  $V$  is the molar volume,  $\gamma$  is the surface tension,  $\theta$  is the contact angle,  $R$  is the gas constant,  $T$  is the temperature, and  $r$  is the radius of curvature of a pore. For the last, consider that a soil comprised of spherical grains  $0.13 \mu\text{m}$  in diameter has a surface area of  $17 \text{ m}^2/\text{g}$ , equivalent to the Viking measurement. Pore radii in this theoretical medium are a few hundredths of a micron. In a heterogeneous soil matching Viking, *Clifford and Hillel* [1983] showed that such a fine-grained component can dominate the surface area.

[40] Taking  $r = 0.03 \mu\text{m}$ ,  $\gamma \cos \theta = 6 \text{ Pa}$  [*Stephens*, 1996] and  $V = 1.8 \times 10^{-5} \text{ m}^3/\text{mol}$ , we find  $P/P_0 = 0.03$  at 250 K. The vapor pressure is further reduced by a factor of 1.5–1.8 by the presence of  $\text{NaClO}_4$  or  $\text{MgCl}_2$  at eutectic compositions (Raoult's Law), so  $P/P_0 \approx 0.02$ .  $P_0 = 95 \text{ Pa}$  at 250 K [*Goff and Gratch*, 1946; *List*, 1984], therefore the vapor pressure over saline water in small pores is  $\sim 1.9 \text{ Pa}$ . Experimentally observed evaporation rates under nominal Mars surface conditions are  $\sim 75 \mu\text{m}/\text{h}$  [*Altheide et al.*, 2009; *Chevrier et al.*, 2009] (extrapolated to 250 K; see also *Clifford and Hillel* [1983]). Assuming evaporation rate is proportional to vapor pressure [*Farmer*, 1976], even a two-order-of-magnitude reduction in vapor pressure still implies evaporation time scales for  $0.03\text{-}\mu\text{m}$  radius pores of about a minute. Consider, however, that water ice is present (and stable) within several cm of the surface. The vapor pressure over water ice is  $1.4 \text{ Pa}$  (e.g., Goff-Gratch equation from *List* [1984]), at the average subsurface temperature 215 K. This is within 35% of the crudely estimated pore water vapor pressure above, and therefore it is likely that diurnal eutectic meltwater in the surficial material at the Phoenix landing site is preserved against evaporation by the vapor pressure of the nearby ice table.

[41] Because adsorption and capillarity depend on similar intermolecular forces, radiation damage to the shallowest regolith (discussed above with respect to its influence on adsorption) could also affect surface tension. The exponential Kelvin equation greatly magnifies the effect of changes in surface tension on vapor pressure, so that simply

doubling the former would decrease the latter to well below the ice vapor pressure, ensuring liquid stability.

## 7. Conclusions

[42] The TECP is so sensitive to regolith-probe coupling that only long-duration measurements can be used for quantitative analysis. Unfortunately, only three such data sets were taken, and all at the Vestri site. Using a library of laboratory permittivity measurements, we identified daytime melting of ice containing either  $\text{MgCl}_2$  or  $\text{NaClO}_4$ . This briny ice is heterogeneous at Vestri as it was identified in only two of the three data sets. We concur with *Zent et al.* [2010] that nighttime  $\text{H}_2\text{O}$  adsorption was detected by TECP, but the total amount of soil-adsorbed water that we infer from laboratory measurements is about one order of magnitude too high. This is an improvement over the two-order-of-magnitude discrepancy in the analytical approach used by Zent and coworkers, but it calls for some difference between Earth and Mars in the dielectric behavior of adsorbed water.

[43] New instrumentation will measure complex permittivity over large bandwidths to better describe materials and charge-transfer mechanisms, i.e., perform in situ dielectric spectroscopy. First is the Permittivity Probe (PP) on the Rosetta comet lander (Philae), which has a bandwidth of 10 Hz – 10 kHz and uses multiple surface electrodes to measure complex permittivity up to 70 cm deep [*Seidensticker et al.*, 2007]. Our own prototype [*Stillman and Grimm*, 2008] will measure up to 100 kHz and has a flexible electrode geometry that will enable investigation to tens of meters. All such in situ dielectric spectroscopy must pay careful attention to calibration and coupling. Further laboratory measurements, especially on radiation-damaged analog materials at Martian surface conditions, will provide dielectric mixing models that could be used to quantify the amounts of ice, adsorbed water, and liquid brines in the subsurface [*Grimm and Stillman*, 2011].

## Appendix A: $\text{Mg}(\text{ClO}_4)_2\text{-H}_2\text{O}$ Eutectic Temperature

[44] The eutectic temperature is clearly discernable while measuring the electrical properties of salty ices (Figure 2) [e.g., *Matsuoka et al.*, 1997; *Grimm et al.*, 2008; *Stillman et al.*, 2010]. We noticed that repeated measurements of  $\text{Mg}(\text{ClO}_4)_2$  yielded a eutectic temperature of  $\sim 216 \text{ K}$ , not  $206 \text{ K}$  as reported by *Pestova et al.* [2005] and *Dobrynina et al.* [1980]. Sample contamination and measurement error was ruled out by obtaining  $\text{Mg}(\text{ClO}_4)_2$  from two different suppliers (Acros-Organics Lot: A0257020 and EMD chemicals Lot: 49217935). We then performed calorimetry on eutectic compositions of both  $\text{Mg}(\text{ClO}_4)_2$  samples and a  $\text{NaClO}_4$  sample (Figure A1). This analysis gave a eutectic temperature of  $216.0 \pm 0.2 \text{ K}$  and  $239.8 \pm 0.2 \text{ K}$  for  $\text{Mg}(\text{ClO}_4)_2$  and  $\text{NaClO}_4$ , respectively. The  $\text{NaClO}_4$  matches perfectly with previous data, while the  $\text{Mg}(\text{ClO}_4)_2$  is 10 K warmer. *Pestova et al.* [2005] measured only while cooling at  $0.3\text{--}1 \text{ K}/\text{min}$ . We infer that the lower apparent eutectic temperature is the result of supercooling, to which solutions with the largest freezing-point depressions are especially vulnerable. *Dobrynina et al.* [1980] measured both during

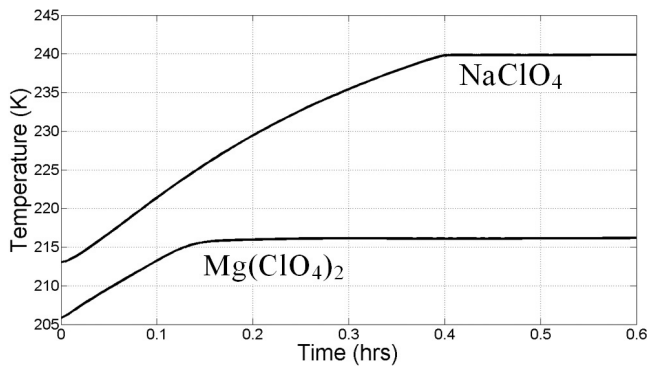


**Figure A1.** Calorimetry of  $\text{Mg}(\text{ClO}_4)_2$  and  $\text{NaClO}_4$  eutectic compositions showed eutectic temperatures of  $216.0 \pm 0.2$  and  $239.8 \pm 0.2$  K, respectively.

cooling and warming but at a rate of 5–10 K/min, whereas our electrical properties measurements were made during warming only at 1 K/min and holding the temperature within  $\pm 0.2$  K during the 30 min measurement and 30 min prior to the measurement. We therefore suggest that incorrect procedures led to these prior lower temperatures.

## Appendix B: TECP

[45] We determined the depth response (Green's function) of the TECP permittivity experiment using numerical modeling (COMSOL Multiphysics 3.5a AC/DC module). The problem is treated as purely electrostatic, i.e., conduction and

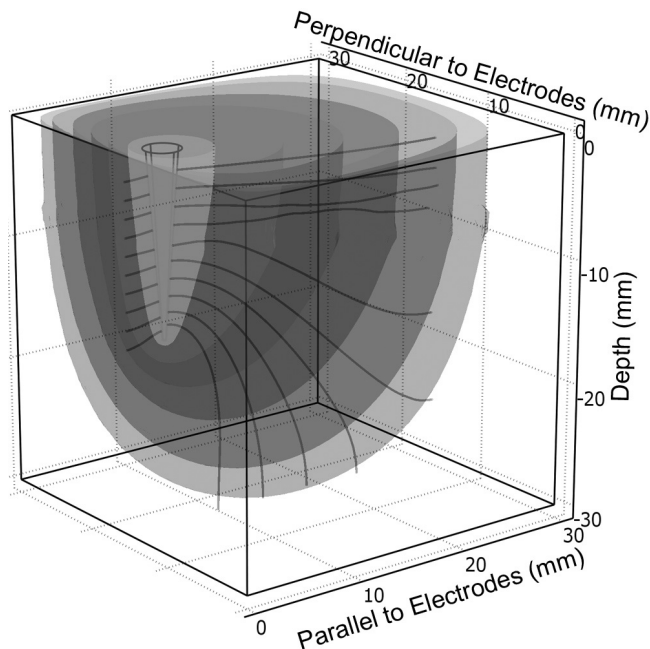


**Figure B1.** Isosurfaces of electric potential (0.5, 0.2, 0.1, 0.05, 0.02, 0.01 V) for TECP permittivity electrode held at 1 V. The second electrode is implicit by symmetry, equidistant from the vertical ground plane nearest to the modeled electrode. Electric field lines are shown only in the plane of the electrodes. The discontinuity due to a thin, high-permittivity test layer at 7.5 mm is evident.

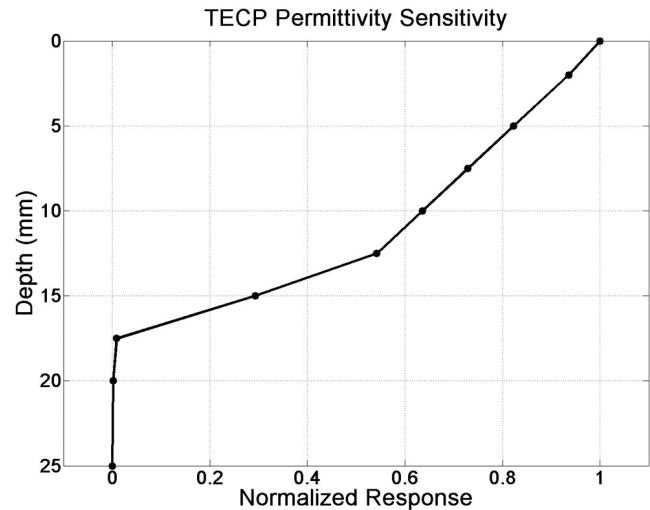


**Figure B2.** Depth sensitivity of the TECP permittivity experiment. A value of zero implies only a background permittivity can be detected; a value of unity implies that local contrasts are fully characterized. The sensitivity is essentially limited to the penetration depth of the electrodes, and the sensitivity at the surface is  $\sim 1.4$  times the mean.

frequency dependence were neglected. A single electrode is modeled as a truncated cone of length 15 mm and basal diameter 3 mm. The second electrode, 7 mm away is implicit by inserting a ground plane at 3.5 mm. The electrode potential is 1 V. The model domain is a 30 mm cube; all boundaries are grounds except the free surface, which is insulating. Results agree to within 10% when the four artificial boundaries are also treated as insulators. The inferred permittivity is proportional to the lumped capacitance of the system. The depth kernels are computed by treating the background as unit permittivity and inserting a thin, high-permittivity layer (Figure B1) at each test depth. The response function is the normalized difference in capacitance between the models with and without the thin layer.

[46] The model results indicate a relatively simple depth function (Figure B2) for the TECP permittivity sensitivity. Sensitivity falls off linearly until just above the bottom of the electrodes, where it turns sharply downward. The sensitivity averaged over the full depth of the electrodes is 0.7, so a thin, near-surface layer of high permittivity has 1.4 times the influence of a uniformly distributed permittivity enhancement.

[47] **Acknowledgments.** This work was funded by the NASA Mars Fundamental Research Program (NNX08AN44G). We thank Mark Bullcock, Doug Cobos, Mike Hecht, Tim Michaels, Scot Rafkin, and Kerry Neal for helpful discussions. This paper was improved by the thorough and constructive review of Antoine Pommerol. An anonymous reviewer focused clarification of the TECP measurements and how corrections were applied.

## References

- Allen, C. C., R. V. Morris, D. J. Lindstrom, M. M. Lindstrom, and J. P. Lockwood (1997), JSC Mars-1: Martian regolith stimulant, *Lunar Planet. Sci.*, *XXVIII*, Abstract 1797.
- Altheide, T., V. Chevrier, C. Nicholson, and J. Denson (2009), Experimental investigation of the stability and evaporation of sulfate and chloride brines on Mars, *Earth Planet. Sci. Lett.*, *282*, 69–78, doi:10.1016/j.epsl.2009.03.002.

- Anderson, D. M., and A. R. Tice (1973), The unfrozen interfacial phase in frozen soil water systems, in *Physical Aspects of Soil Water and Salts in Ecosystems*, *Ecol. Stud.*, vol. 4, pp. 107–124, Springer, London.
- Arvidson, R. E., et al. (2009), Results from the Mars Phoenix Lander Robotic Arm experiment, *J. Geophys. Res.*, *114*, E00E02, doi:10.1029/2009JE003408.
- Asay, D. B., and S. H. Kim (2005), Evolution of the adsorbed water layer structure on silicon oxide at room temperature, *J. Phys. Chem. B*, *109*(35), 16,760–16,763, doi:10.1021/jp053042o.
- Ballou, E. V., P. C. Wood, T. Wydeven, M. E. Lehwalt, and R. E. Mack (1978), Chemical interpretation of Viking lander 1 life detection experiment, *Nature*, *271*, 644–645, doi:10.1038/271644a0.
- Beck, P., A. Pommerol, B. Schmitt, and O. Brissaud (2010), Kinetics of water adsorption on minerals and the breathing of the Martian regolith, *J. Geophys. Res.*, *115*, E10011, doi:10.1029/2009JE003539.
- Bittelli, M., M. Flury, and G. S. Campbell (2003), A thermodielectric analyzer to measure the freezing and moisture characteristic of porous media, *Water Resour. Res.*, *39*(2), 1041, doi:10.1029/2001WR000930.
- Chevrier, V. F., J. Hanley, and T. S. Altheide (2009), Stability of perchlorate hydrates and their liquid solutions at the Phoenix landing site, Mars, *Geophys. Res. Lett.*, *36*, L10202, doi:10.1029/2009GL037497.
- Chretien, A., and R. Kohlmuller (1966), Perchlorate de sodium, in *Nouveau Traite de Chimie Minerale*, vol. 2(1), *Sodium and Lithium*, edited by P. Pascal, pp. 344–354, Masson and Cie, Paris.
- Clifford, S. M., and D. Hillel (1983), The stability of ground ice in the equatorial region of Mars, *J. Geophys. Res.*, *88*, 2456–2474, doi:10.1029/JB088iB03p02456.
- Cull, S., R. E. Arvidson, R. V. Morris, M. Wolff, M. T. Mellon, and M. T. Lemmon (2010), Seasonal ice cycle at the Mars Phoenix landing site: 2. Postlanding CRISM and ground observations, *J. Geophys. Res.*, *115*, E00E19, doi:10.1029/2009JE003410.
- Dash, J. G., A. W. Rempel, and J. S. Wettlaufer (2006), The physics of premelted ice and its geophysical consequences, *Rev. Mod. Phys.*, *78*, 695–741, doi:10.1103/RevModPhys.78.695.
- Dobrynina, T. A., A. M. Chernyshova, N. A. Akhapkina, and V. Y. Rosolovskii (1980), Fusion diagram of the magnesium perchlorate-water system, *Russ. J. Inorg. Chem.*, *25*, 2233–2236.
- Fanale, F. P., and W. A. Cannon (1979), Mars: CO<sub>2</sub> adsorption and capillary condensation on clays: Significance for volatile storage and atmospheric history, *J. Geophys. Res.*, *84*(8), 404–408, 414.
- Farmer, C. B. (1976), Liquid water on Mars, *Icarus*, *28*, 279–289, doi:10.1016/0019-1035(76)90038-5.
- Goff, J. A., and S. Gratch (1946), Low-pressure properties of water from –160 to 212 F, paper presented at the 52nd Annual Meeting, Am. Soc. of Heating and Ventilating Eng., New York.
- Gregory, B. L., and C. W. Gwyn (1974), Radiation effects on semiconductor devices, *Proc. IEEE*, *62*, 1264–1273, doi:10.1109/PROC.1974.9605.
- Grimm, R. E., and D. E. Stillman (2011), Progress in prospecting for near-surface H<sub>2</sub>O on the Moon and Mars with dielectric spectroscopy, *Lunar Planet. Sci.*, *42nd*, 2550.
- Grimm, R. E., D. E. Stillman, S. F. Dec, and M. Bullock (2008), Low-frequency electrical properties of polycrystalline saline ice and salt hydrates, *J. Phys. Chem. B*, *112*, 15,382, doi:10.1021/jp8055366.
- Haberle, R. M., C. P. McKay, J. Schaeffer, N. A. Cabrol, E. A. Grin, and A. P. Zent (2001), On the possibility of liquid water on present-day Mars, *J. Geophys. Res.*, *106*, 23,317–23,326, doi:10.1029/2000JE001360.
- Hecht, M. H., et al. (2009), Detection of perchlorate and the soluble chemistry of Martian soil: Findings from the Phoenix Mars Lander, *Science*, *325*, 64–67.
- Heet, T. L., R. E. Arvidson, S. C. Cull, M. T. Mellon, and K. D. Seelos (2009), Geomorphic and geologic settings of the Phoenix Lander mission landing site, *J. Geophys. Res.*, *114*, E00E04, doi:10.1029/2009JE003416.
- Jakosky, B. M., K. H. Nealson, C. Bakermans, R. E. Ley, and M. T. Mellon (2003), Subfreezing activity of microorganisms and the potential habitability of Mars' polar regions, *Astrobiology*, *3*(2), 343–350, doi:10.1089/153110703769016433.
- Jonscher, A. K. (1978), Low-frequency dispersion in carrier-dominated dielectrics, *Philos. Mag. B*, *38*, 587–601, doi:10.1080/13642817808246336.
- Kauzmann, W. (1942), Dielectric relaxation as a chemical rate process, *Rev. Mod. Phys.*, *14*, 12–44, doi:10.1103/RevModPhys.14.12.
- Linke, W. F. (1965), *Solubilities of Inorganic and Metal Organic Compounds*, vol. II, 4th ed., 1914 pp., Am. Chem. Soc., Washington, D. C.
- List, R. J. (1984), *Smithsonian Meteorological Tables*, 6th ed., 350 pp., Smithsonian Inst. Press, Washington, D. C.
- Marion, G. M., D. C. Catling, K. J. Zahnle, and M. W. Claire (2010), Modeling aqueous perchlorate chemistries with applications to Mars, *Icarus*, *207*, 675–685, doi:10.1016/j.icarus.2009.12.003.
- Matsuoka, T., S. Fujita, and S. Mae (1997), Dielectric properties of ice containing ionic impurities at microwave frequencies, *J. Phys. Chem.*, *101*, 6219–6222, doi:10.1021/jp9631590.
- McCafferty, E., and A. C. Zettlemoyer (1971), Adsorption of water vapour on alpha-Fe<sub>2</sub>O<sub>3</sub>, *Discuss. Faraday Soc.*, *52*, 239, doi:10.1039/d19715200239.
- McKay, D. S., J. L. Carter, W. W. Boles, C. C. Allen, and J. H. Allton (1997), JSC-1: A new lunar regolith simulant, *Lunar Planet. Sci.*, *XXIV*, 963.
- Mellon, M. T., et al. (2009), Ground ice at the Phoenix landing site: Stability state and origin, *J. Geophys. Res.*, *114*, E00E07, doi:10.1029/2009JE003417.
- Olhoeft, G. R., and D. W. Strangway (1975), Dielectric properties of the first 100 meters of the Moon, *Earth Planet. Sci. Lett.*, *24*, 394–404, doi:10.1016/0012-821X(75)90146-6.
- Olhoeft, G. R., A. L. Frisillo, D. W. Strangway, and H. Sharpe (1974), Temperature dependence of electrical conductivity and lunar temperatures, *Earth Moon Planets*, *9*, 79–87, doi:10.1007/BF00565394.
- Pestova, O. N., L. A. Myund, M. K. Khripun, and A. V. Prigaro (2005), Polythermal study of the systems M(ClO<sub>4</sub>)<sub>2</sub> – H<sub>2</sub>O (M<sup>2+</sup> = Mg<sup>2+</sup>, Ca<sup>2+</sup>, Sr<sup>2+</sup>, Ba<sup>2+</sup>), *Russ. J. Appl. Chem.*, *78*, 409–413, doi:10.1007/s11167-005-0306-z.
- Pommerol, A., B. Schmitt, P. Beck, and O. Brissaud (2009), Water sorption on Martian regolith analogs: Thermodynamics and near-infrared reflectance spectroscopy, *Icarus*, *204*, 114–136, doi:10.1016/j.icarus.2009.06.013.
- Rennó, N. O., et al. (2009), Possible physical and thermodynamical evidence for liquid water at the Phoenix landing site, *J. Geophys. Res.*, *114*, E00E03, doi:10.1029/2009JE003362.
- Rubin, Y., and S. S. Hubbard (Eds.) (2005), *Hydrogeophysics*, 523 pp., Springer, Dordrecht, Netherlands, doi:10.1007/1-4020-3102-5.
- Seidensticker, J. K., et al. (2007), SESAME—An experiment of the Rosetta Lander Philae: Objectives and general design, *Space Sci. Rev.*, *128*, 301–337, doi:10.1007/s11214-006-9118-6.
- Shabtaie, S., and C. R. Bentley (1994), Unified theory of electrical conduction in firm and ice: Site percolation and conduction in snow and firm, *J. Geophys. Res.*, *99*, 19,757–19,769, doi:10.1029/94JB01510.
- Shahidi, M., J. B. Hasted, and A. K. Jonscher (1975), Electrical properties of dry and humid sand, *Nature*, *258*, 595–597, doi:10.1038/258595a0.
- Shivola, A. (1999), *Electromagnetic Mixing Formulas and Applications*, 284 pp., IEE, London.
- Stephens, D. B. (1996), *Vadose Zone Hydrology*, 347 pp., CDC Press, New York.
- Stillman, D. E., and R. E. Grimm (2008), Electrical properties of ice and implications for solar system exploration, *Lunar Planet. Sci.*, *XXXIX*, Abstract 2277.
- Stillman, D. E., and R. E. Grimm (2011), Radar penetrates only the youngest geological units on Mars, *J. Geophys. Res.*, *116*, E03001, doi:10.1029/2010JE003661.
- Stillman, D. E., R. E. Grimm, and S. F. Dec (2010), Low-frequency electrical properties of ice-silicate mixtures, *J. Phys. Chem. B*, *114*, 6065–6073, doi:10.1021/jp9070778.
- Tamppari, L. K., et al. (2010), Phoenix and MRO coordinated atmospheric measurements, *J. Geophys. Res.*, *115*, E00E17, doi:10.1029/2009JE003415.
- Topp, G. C., J. L. Davis, and A. P. Annan (1980), Electromagnetic determination of soil water content: Measurements in coaxial transmission lines, *Water Resour. Res.*, *16*, 574–582, doi:10.1029/WR016i003p00574.
- Zent, A. P., and R. C. Quinn (1995), Simultaneous adsorption of CO<sub>2</sub> and H<sub>2</sub>O under Mars-like conditions and application to the evolution of the Martian climate, *J. Geophys. Res.*, *100*, 5341–5349, doi:10.1029/94JE01899.
- Zent, A. P., M. H. Hecht, D. R. Cobos, G. S. Campbell, C. S. Campbell, G. Cardell, M. C. Foote, S. E. Wood, and M. Mehta (2009), Thermal and Electrical Conductivity Probe (TECP) for Phoenix, *J. Geophys. Res.*, *114*, E00A27, doi:10.1029/2007JE003052.
- Zent, A. P., M. H. Hecht, D. R. Cobos, S. E. Wood, T. L. Hudson, S. M. Milkovich, L. P. DeFlores, and M. T. Mellon (2010), Initial results from the thermal and electrical conductivity probe (TECP) on Phoenix, *J. Geophys. Res.*, *115*, E00E14, doi:10.1029/2009JE003420.
- Zhou, L. (2002), Adsorption isotherms for the supercritical region, in *Adsorption: Theory, Modeling, and Analysis*, edited by J. Toth, pp. 211–250, Marcel Dekker, New York.

R. E. Grimm and D. E. Stillman, Department of Space Studies, Southwest Research Institute, 1050 Walnut, Ste. 300, Boulder, CO 80302, USA. (dstillman@boulder.swri.edu)